A comprehensive lift force model for deformable bubbles rising in moderate shear flows

International Journal of Multiphase Flow 187 (2025) 105166

Contents lists available at ScienceDirect

International Journal of Multiphase Flow

journal homepage: www.elsevier.com/locate/ijmulflow

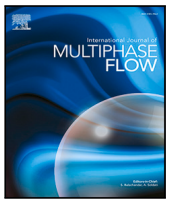

Express Track Article

A comprehensive lift force model for deformable bubbles rising in moderate shear flows

Niklas Hidman *, Henrik Ström, Gaetano Sardina, Srdjan Sasic

Department of Mechanics and Maritime Sciences, Chalmers University of Technology, Gothenburg, Sweden

ARTICLE INFO

Keywords:
Bubble dynamics
Lift force
Shear flow

ABSTRACT

We provide comprehensive regression models for the lift force coefficient C_L and the terminal relative velocity for clean deformable bubbles in moderate shear flows. The models are expressed as functions of the a priori known Galilei (Ga) and Eötvös (Eo) numbers, eliminating the need for additional sub-models to predict, for example, the bubble shape. The proposed models are developed for a wide range of governing parameters (approximately $(3 < Ga < 10000)$ and $(Eo < 20)$) and show good agreement with the existing numerical and experimental data. This robustness makes the models highly applicable to most practical gas–liquid systems. The C_L-model is particularly suited for moderate-to-high non-dimensional shear rates $Sr = O(0.01-0.1)$, where the lift force is significant compared to other hydrodynamic forces.

1. Introduction

Bubbles rising in a shear flow experience a shear-induced lift force in a direction perpendicular to their relative motion. This lift force governs the spatial distribution of bubbles in many important applications such as bubbly pipe flows and bubble column reactors. It is therefore important to have accurate models for the lift force in multi-fluid models and bubble tracking methods to correctly predict the dynamics of gas–liquid systems (Mudde, 2005; Lucas et al., 2020; Ertekin et al., 2021).

The lift force is governed by the complex interaction of four lift force mechanisms that can be explained by their distinct bubble-induced vorticity fields (Hidman et al., 2022). The generation of these vorticity fields generally depends on the bubble size and shape, the gas–liquid properties and the shear rate. Consequently, any of the four mechanisms may dominate the net lift force depending on those conditions. In addition, the lift force induced by the mechanisms scales differently with the governing parameters. It is, therefore, very difficult to develop universally applicable lift force models based on analytical solutions or physical arguments.

Additionally, depending on the mechanism that governs the net lift force, the lift force may act towards the side of the bubble either with the highest or the lowest relative liquid velocity. This phenomenon is commonly known as lift force reversal (Tomiyama et al., 2002; Adoua et al., 2009; Hayashi et al., 2021). For example, in bubbly pipe flows, the lift force pushes the bubbles either towards the pipe walls or the pipe centre (Lucas et al., 2001; Lucas and Tomiyama, 2011). The lift force also influences the flow stability in bubble columns because the force direction determines whether the bubbles cluster or spread uniformly (Lucas et al., 2005; Mazzitelli and Lohse, 2009).

Reliable and universal lift force models need to consider the influence of all four mechanisms and accurately predict the important lift force reversal phenomenon. These challenges and insufficient experimental data have so far hindered the development of reliable and universally applicable lift force models. Although the lift force acting on spherical bubbles is well understood (Legendre and Magnaudet, 1998), there are still no general models for deformed bubbles (Hayashi et al., 2020). To the best of the authors' knowledge, no lift force model is developed for all relevant scenarios of spherical to very deformed bubbles in low to high viscosity liquids.

In this work we provide a comprehensive lift force regression model (henceforth referred to as a model) based on our previous work (Hidman et al. (2022) with the inclusion of more data points covering a wider range of the governing parameters, a new regression method and more thorough validation) and available numerical and experimental results from the literature. By non-dimensionalizing the problem with a priori known parameters, we first identify suitable non-dimensional governing parameters and then analyse their influence on the lift force. Based on our findings, we develop a lift force model for a very wide range of governing parameters. This facilitates the practical use of our model (alleviating the need of switching between different models depending upon the specific flow condition) and avoids the need of additional sub-models (to predict, for example, the bubble shape). In

* Corresponding author.
E-mail address: niklas.hidman@chalmers.se (N. Hidman).

https://doi.org/10.1016/j.ijmultiphaseflow.2025.105166
Received 23 December 2024; Received in revised form 4 February 2025; Accepted 7 February 2025
Available online 21 February 2025

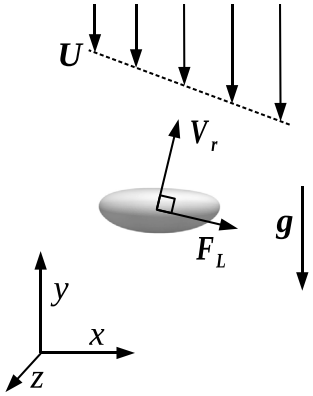

Fig. 1. Illustration of the studied flow configuration.

addition, we provide a model for the terminal relative velocity of the bubble, also based on findings from the literature and a-priori known parameters.

2. Problem description

We consider a deformable and freely moving bubble rising in a linear shear flow, shown schematically in Fig. 1. Here, the undisturbed liquid shear rate is $\omega_\infty = dU_y/dx < 0$. The shear-induced lift force is typically formulated as (Žun, 1980; Auton, 1987; Drew and Lahey, 1987)

$$\boldsymbol{F}_L = -C_L \Omega_g \rho_l \boldsymbol{V}_r \times \boldsymbol{\omega}_U , \tag{1}$$

where C_L is the lift force coefficient, Ω_g is the bubble volume, ρ_l is the liquid density, $\boldsymbol{V}_r = \boldsymbol{V} - \boldsymbol{U}$ is the relative velocity between the bubble $\boldsymbol{V}$ and the undisturbed liquid $\boldsymbol{U}$ and $\boldsymbol{\omega}_U = \boldsymbol{\nabla} \times \boldsymbol{U}$ is the undisturbed liquid vorticity, all evaluated at the bubble position. With this definition, the lift force is positive in the direction of the highest relative liquid velocity (here, in the positive x-direction). Considering C_L as the only unknown variable on the RHS of Eq. (1), the objective of the present study can be formulated as finding a model for C_L based on the governing parameters.

To determine convenient governing parameters, we non-dimensionalize the governing equations (two-phase Navier–Stokes) and boundary conditions ($U_y = \omega_\infty x$) with the (a-priori known) spherical-equivalent bubble diameter D, gravitational acceleration g and the liquid density ρ_l (see Appendix A). This yields the following set of five dimensionless parameters that completely describes the problem of a bubble rising in a linear shear flow (Tripathi et al., 2014; Hidman et al., 2022):

$$\text{Galilei number: } Ga = \frac{\rho_l \sqrt{gD}\, D}{\mu_l}, \tag{2}$$

$$\text{Eötvös number: } Eo = \frac{\rho_l g D^2}{\sigma}, \tag{3}$$

$$\text{dimensionless shear rate: } Sr = \frac{|\omega_\infty| D}{\sqrt{gD}}, \tag{4}$$

$$\text{density ratio: } \rho_r = \frac{\rho_l}{\rho_g}, \tag{5}$$

$$\text{dynamic viscosity ratio: } \mu_r = \frac{\mu_l}{\mu_g}, \tag{6}$$

where σ is the surface tension, $|\omega_\infty|$ is the absolute value of the upstream undisturbed vorticity and the subscripts l and g represent liquid and gas properties, respectively. Typical density and viscosity ratios are approximately $\rho_r = 1000$ and $\mu_r = 100$. However, at ratios above 50, the pressure and viscous forces acting on the bubble interface by the gas are practically negligible compared to those forces acting on the interface by the liquid (Bunner and Tryggvason, 2002). Therefore, at the practically relevant ratios (above 50), the lift force becomes independent of ρ_r and μ_r. In this work, we consider only ratios well above 50. These considerations leave a set of three dimensionless parameters (Ga, Eo, Sr) that govern the present problem. Considering the different behaviours of bubble dynamics and the lift force, we categorize the Galilei number as low for $Ga \leq O(1)$, moderate for $Ga = O(10)$, and high for $Ga \geq O(100)$. The Eötvös number is considered low when $Eo \leq O(0.1)$, moderate when $Eo = O(1)$, and high when $Eo \geq O(10)$. Additionally, the dimensionless shear rate is deemed low for $Sr \leq O(0.001)$, moderate for $Sr = O(0.01)$, and high for $Sr \geq O(0.1)$.

The commonly used Reynolds-, $Re = \rho_l |\overline{V}_r| D/\mu_l$, and Weber-, $We = \rho_l |\overline{V}_r|^2 D/\sigma$, numbers are related to Ga and Eo through the Froude number as $Fr = |\overline{V}_r|/\sqrt{gD} = Re/Ga = \sqrt{We/Eo}$. Here, $|\overline{V}_r|$ is the Euclidian norm of the quasi-steady terminal relative velocity of the bubble (typically obtained by averaging over several oscillation periods in for example, quasi-steady zig-zagging bubbles (Cano-Lozano et al., 2016)). Since $|\overline{V}_r|$ is unknown a priori, the Ga and Eo-numbers are a more convenient choice to describe the present problem. Assuming a weak influence of Sr on Fr, the latter becomes a function $Fr(Ga, Eo)$ that can be used to map between any function $f(Ga, Eo) \leftrightarrow f(Re, We)$. A model for $Fr(Ga, Eo)$ is given in Section 3. It is also worth noting that the well-known Morton number is related to the governing parameters as $Mo = g\mu_l^4/\rho_l \sigma^3 = Eo^3/Ga^4$.

The lift force coefficient has been analytically derived for the special cases of a spherical bubble in very viscous (low Ga) and inviscid liquids ($Ga \to \infty$). In very viscous flows, C_L becomes (Saffman, 1965; Legendre and Magnaudet, 1997, 1998)

$$C_{L,Saffman} = \frac{6}{\pi^2} (ReSr_V)^{-1/2} J(\epsilon), \tag{7}$$

where $Sr_V = (|\omega_\infty| D)/|\overline{V_{rel}}|$, $\epsilon = (Sr_V/Re)^{1/2}$ and $J(\epsilon)$ is the value of a three-dimensional integral (McLaughlin, 1991). For a spherical bubble in a weakly sheared inviscid flow, Auton (1987) derived the famous result

$$C_{L,\infty} = 0.5. \tag{8}$$

These analytical solutions show that C_L for a spherical bubble can have either a complex dependency on Sr ($C_{L,Saffman}$) or be independent of Sr ($C_{L,\infty}$), depending on the Ga-number. For deformable (non-spherical) bubbles, there are no analytical solutions and C_L is, in general, a function of all the governing parameters $C_L(Ga, Eo, Sr)$.

To develop a practically relevant regression model for C_L, we choose here to focus on moderate-to-high shear rates of $Sr = O(0.01) - O(0.1)$, where the magnitude of the lift force is typically comparable to other forces, such as the drag. Most of the numerical and experimental data in the literature are also obtained at these values of shear rates and do not exhibit any clear trends. The model developed in this work therefore does not include a shear rate dependence. However, C_L generally depends on Sr at low Ga conditions (Eq. (7)), and at moderate-to-high Eo (non-spherical bubble shapes) and high Ga conditions (Adoua et al., 2009; Hidman et al., 2022). For such conditions, and at $Sr < O(0.01)$, the model developed in this work is expected to be less accurate.

3. Terminal velocity model

Numerical and experimental observations of C_L are typically presented based on either the characteristic velocity scale $\sqrt{gD}$ (Ga, Eo-numbers) or the relative terminal velocity $|\overline{V}_r|$ (Re, We-numbers). To express all observations of C_L as a function of our governing parameters (Ga, Eo), we thus need a mapping function (the velocity scale relation) $Fr(Ga, Eo) = |\overline{V}_r|/\sqrt{gD}$.

Here, we use the values for $|\overline{V}_r|$ presented in Cano-Lozano et al. (2016), Aoyama et al. (2017), Ziegenhein et al. (2018), Hidman et al. (2022) for bubbles rising in quiescent and linear shear flows. The data span ranges of approximately $(3 < Ga < 1500)$ and $(0.1 < Eo < 100)$. All data points are shown in Fig. 2 together with the fitted surface defined

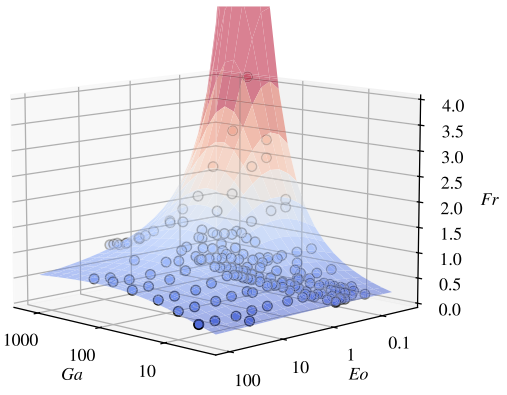

Fig. 2. Non-dimensional terminal relative bubble velocity Fr in the $Ga-Eo$ phase space. The included data points and the fitted surface Fr^{reg} are coloured by the Fr-value where dark blue is $Fr=0$ and dark red is $Fr=4$. (For interpretation of the references to colour in this figure legend, the reader is referred to the web version of this article.)

by

$$Fr^{reg}=\frac{0.17+1.16x-0.2y+0.3xy-0.15x^2+0.06y^2}{4.2-3x-0.4y+0.69xy+0.73x^2+0.4y^2}, \tag{9}$$

where $x=\log_{10}(Ga)$ and $y=\log_{10}(Eo)$. The absolute standard deviation is $\sigma_{Fr}=0.056$ and the coefficient of determination $R^2=0.98$ between the regression model and the data points. The conformity of the data sets and the good fit to the smooth surface suggest that the influence of Sr on $|\overline{V}_r|$ is small. If $|\overline{V}_r|$ were significantly dependent on Sr, we would expect more scatter in the data and not such a good collapse on the Fr^{reg}-surface since the data are obtained in both quiescent and in shear flows with various shear rates. This observation agrees with the numerical studies of Adoua et al. (2009) and Dijkhuizen et al. (2010), where the drag force and bubble shape are practically constant with the shear rate, in the range of moderate shear rates considered here. In general, $Fr=O(1)$ indicates that the velocity scale $\sqrt{gD}$ is a suitable characteristic velocity for buoyancy-driven deformable and freely moving bubbles.

4. Lift force model

To develop our model, we include numerical and experimental values of C_L at $Sr=O(0.01)-O(0.1)$ from the works of Dijkhuizen et al. (2010), Aoyama et al. (2017), Feng and Bolotnov (2017), Ziegenhein et al. (2018), Hessenkemper et al. (2021), Hidman et al. (2022) spanning ranges of approximately $(3<Ga<1700)$ and $(0.07<Eo<20)$. We also include the numerical results of Legendre and Magnaudet (1998) obtained for fixed spherical bubbles. The spherical shape is obtained asymptotically in the limit of very high surface tension ($Eo\to 0$). Here, this shape is approximated by having a very low but non-zero $Eo=0.001$ to facilitate the description of the results in the log–log space. Having $Eo<0.001$ is not expected to significantly influence C_L since the bubble shape is already close to that of a sphere in the relevant ranges of the governing parameters (Cano-Lozano et al., 2013). The choice of $Eo=0.001$ here is arbitrary but also a reasonable lower limit of practically relevant Eo-numbers. This is indicated by the Mo-number lines in Fig. 3 (for water and mercury, where the latter has an exceptionally low $Mo=O(10^{-14})$ due to its high density and surface tension but low viscosity) that intersects $Eo=0.001$ only at low Ga-numbers. Since the bubbles are close to spherical in the range of $0.001<Eo<0.1$, we expect only minor changes to C_L in this interval. The lack of data points between $0.001<Eo<0.1$ is therefore not expected to significantly influence the accuracy of the model proposed here. Where necessary, we use the model of Eq. (9) to map the results reported for Re to the corresponding Ga-value. The data points and a fitted C_L-surface are shown in Fig. 3. The C_L-surface is obtained by fitting the ratio of two third-order surfaces with the optimal coefficients given by

$$C_L^{reg}=\frac{4.4-12x-7.9y+0.4y^2-0.65y^3+17xy-2xy^2+10x^2-11.8x^2y-x^3}{-2.6-3y-1.17y^2-0.38y^3+10x+11xy+2.7xy^2-7x^2-10x^2y+5.2x^3}, \tag{10}$$

where $x=\log_{10}(Ga)$ and $y=\log_{10}(Eo)$. The absolute standard deviation is $\sigma_{C_L}=0.09$ and the coefficient of determination $R^2=0.99$ between the regression model and the data points that show some scatter. It is interesting to note that the best fit was obtained by fitting the above surface to the C_L-values in the $Ga-Mo$ phase space (probably since most data series are obtained at constant Mo-numbers) and then substituting back to the $Ga-Eo$ phase space. The set of (Mo,Ga) can indeed be obtained as the governing parameters provided that the problem is non-dimensionalized using (ρ_l,μ_l,g) instead of (ρ_l,D,g) used in this study (as outlined in Appendix A).

As shown in Fig. 3, C_L^{reg} exhibits steep gradients $(\partial C_L^{reg}/\partial Ga)$ at $Ga\lessapprox 3$. More data is needed to accurately fit the model in this high-gradient region, and C_L^{reg} is, therefore, likely less accurate at $Ga\lessapprox 3$ in general. Similarly, for high Eo-conditions, there is a steep negative slope of $\partial C_L^{reg}/\partial Eo$ that makes the model less accurate at $Eo\gtrapprox 10$. Still, for spherical bubbles (low Eo), C_L^{reg} is in good agreement with the results of Legendre and Magnaudet (1998) with the lowest $Ga\approx 1$, and, at high Ga and low Eo, the model is close to the analytical solution of $C_{L,\infty}=0.5$ valid for spherical bubbles in inviscid flow (Auton, 1987).

The Eq. (10) is an extension of the regression model proposed in Hidman et al. (2022). Here, we include the dataset from that work and from Legendre and Magnaudet (1998) that allows the expansion of the fitted parameter ranges to include spherical bubbles (represented as $Eo=0.001$ where the analytical solution by Saffman (1965), Legendre and Magnaudet (1997) and Auton (1987) are valid) and (high Eo, low Ga)-conditions where the A-mechanism dominates (Hidman et al., 2022). In this work, we also improve the accuracy of the C_L-model by the aforementioned fitting in the (Mo,Ga) phase-space, provide more validation and further discuss the limitation of the model. Finally, here we also develop a regression model for C_L based on the alternative set of the (Re,We) governing parameters in Appendix B. Although these parameters are not known a priori (since they are based on the relative quasi-steady terminal velocity and not the instantaneous relative velocity) they are more conventional in, for example, CFD-codes. For convenience, we therefore provide the $C_L^{reg}(Re,We)$ (Eq. (B.2)) that show similar trends and accuracy as $C_L^{reg}(Ga,Eo)$ in Eq. (10).

4.1. Comparison with previous studies

Fig. 4(a) compares the predicted C_L^{reg} from Eq. (10) with data from the literature (as specified in Section 4). For verification, we also include the measurements of Lee and Lee (2020) that were not used to fit Eq. (10). In total, 204 data points are included here. About 77% of the data is predicted by C_L^{reg} with less than ± 0.1 absolute deviation, and 93% of the data with less than ± 0.2 absolute deviation (indicated as dashed lines in Fig. 4(a)).

A direct comparison between the predicted C_L^{reg} and the data sets from the literature is provided in Fig. 4(b) for the experiments in Aoyama et al. (2017), in Fig. 5 for the numerical results of Dijkhuizen et al. (2010) and in Fig. 6 for the data in Ziegenhein et al. (2018), Hessenkemper et al. (2021), Feng and Bolotnov (2017), Hidman et al. (2022), Legendre and Magnaudet (1998) and Lee and Lee (2020). Here we observe fair quantitative agreement with all data sets and that the correct trends are captured in the wide parameter ranges of $(3<Ga<10000)$ and $(Eo<20)$ considered here. It should be noted again that C_L^{reg} is based on a priori known parameters and not dependent on any sub-models. This is in contrast to most C_L-models proposed in the literature

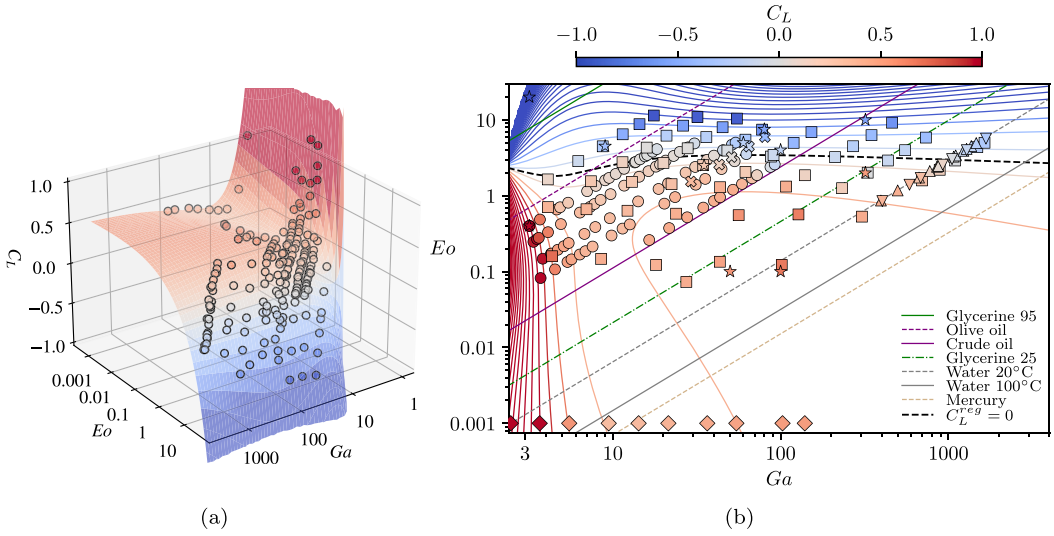

Fig. 3. (a): 3D-view of the included data points and the fitted surface C_L^{reg} (Eq. (10)) coloured by the C_L-value. (b): Data points and contours of C_L^{reg} in the (Ga, Eo)-phase-space together with constant $Mo = Eo^3/Ga^4$-number lines for various relevant liquids (where the glycerine concentration refers to a water–glycerine mixture). The black dashed line is the predicted C_L^{reg}=0-isoline that indicates where the sign of C_L changes. The markers in (b) represent: ● (Aoyama et al., 2017), ■ (Dijkhuizen et al., 2010), ▲ (Ziegenhein et al., 2018), ▼ (Hessenkemper et al., 2021), ✖ (Feng and Bolotnov, 2017), ★ (Hidman et al., 2022) and ◆ (Legendre and Magnaudet, 1998). The contour colour scale are the same in (a) and (b).

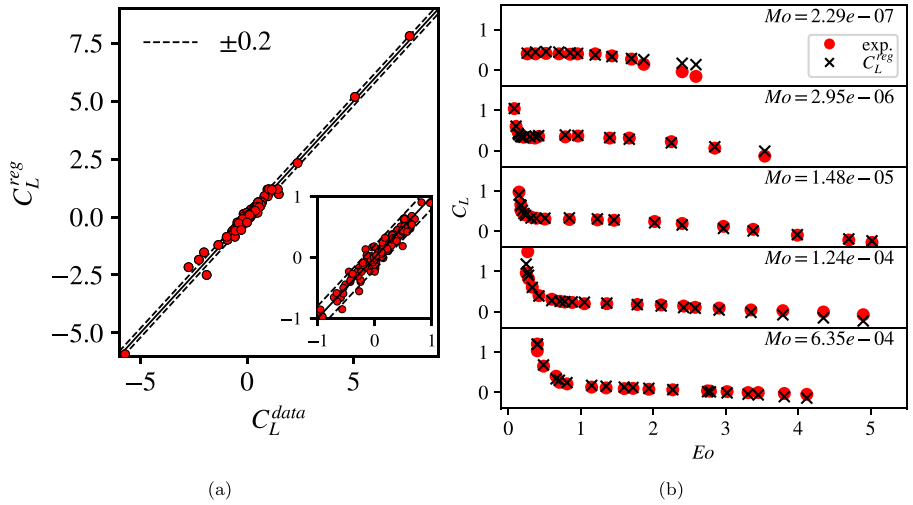

Fig. 4. (a): Comparison of the predicted C_L^{reg} to the C_L^{data} obtained from the literature. (b): Comparison to the experimental results of Aoyama et al. (2017).

that typically focus on relatively narrow parameter ranges (for example, the well-known model by Tomiyama et al. (2002) was developed for approximately ($6 < Ga < 88$) and ($1.4 < Eo < 5.7$)), and/or, the models are based on the deformed bubble shape that is generally unknown a priori and requires further models to be practically useful (for example the informative models of Hayashi et al. (2020, 2021) developed using physical arguments).

5. Conclusions

This paper provides comprehensive and accurate regression models for the lift force coefficient C_L (Eq. (10)) and the non-dimensional terminal relative velocity Fr (Eq. (9)) for clean deformable bubbles rising in moderate shear flows. The models are based on a priori known non-dimensional governing parameters (the Galilei Ga and Eötvös Eo-numbers) without the need for additional models to predict the bubble shape. The influence of the bubble shape on C_L and Fr is included implicitly by Ga and Eo. The C_L and Fr-models are developed for a very wide range of the governing parameters (approximately ($3 < Ga < 10000$) and ($Eo < 20$)) and show good agreement with available numerical and experimental data from the literature. These features make the proposed models useful in most practically relevant systems such as bubbly pipe flows and bubble columns, where the relative velocity between the bubble and liquid phase is induced by gravity (buoyancy). If the relative velocity is induced by other means (e.g. an external electrical field) it is less clear how the proposed models would perform. For convenience, we also provide a model for C_L (Eq. (B.2)) based on an alternative set of the (Re, We) governing parameters (that are typically not known a priori) since these variables are more conventional in, for example, CFD-codes.

The proposed C_L-model is developed for moderate-to-high shear rates of about $Sr = O(0.01 - 0.1)$. This study however motivates further investigations on the influence of Sr on C_L. With more such data, the models proposed here can be extended to include shear rate effects on C_L. The study also motivates more fundamental research on the different lift force mechanisms to provide a better physical

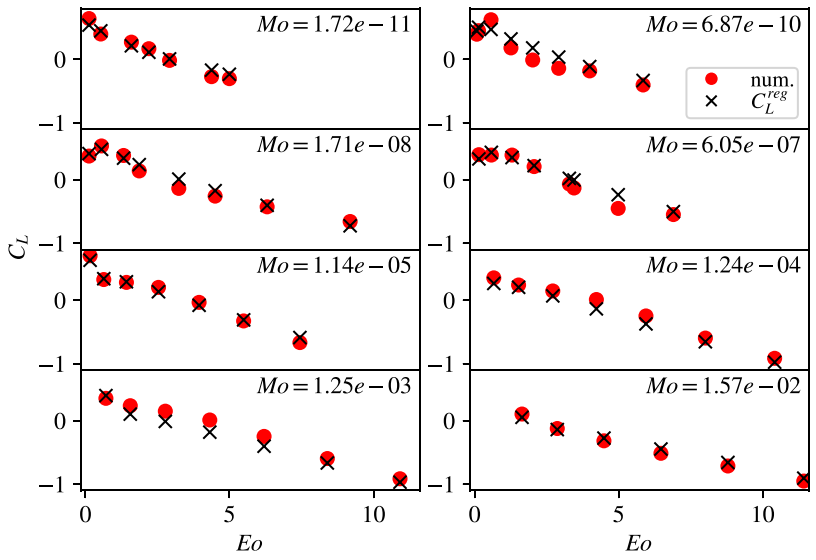

Fig. 5. Comparison of the predicted C_L^{reg} to the numerical results of Dijkhuizen et al. (2010).

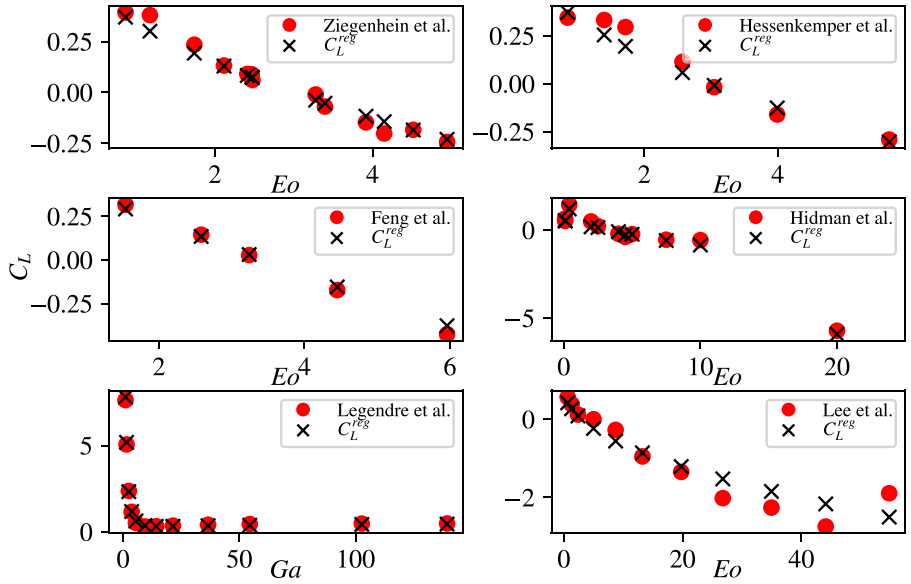

Fig. 6. Comparison of the predicted C_L^{reg} to the experimental results of Ziegenhein et al. (2018), Hessenkemper et al. (2021), Lee and Lee (2020) and the numerical results of Legendre and Magnaudet (1998), Feng and Bolotnov (2017), Hidman et al. (2022).

understanding (and predictions) of the lift force in the entire range of the relevant governing parameters.

CRediT authorship contribution statement

Niklas Hidman: Writing – original draft, Visualization, Validation, Methodology, Investigation, Formal analysis, Data curation, Conceptualization. **Henrik Ström:** Writing – review & editing, Supervision, Conceptualization. **Gaetano Sardina:** Writing – review & editing, Supervision, Resources, Project administration, Funding acquisition, Conceptualization. **Srdjan Sasic:** Writing – review & editing, Supervision, Conceptualization.

Funding sources

This work was supported by the Swedish Research Council (Vetenskapsrådet), grant VR 2017-05031.

Declaration of competing interest

The authors declare that they have no known competing financial interests or personal relationships that could have appeared to influence the work reported in this paper.

Appendix A. Non-dimensional governing equations

We non-dimensionalize all variables using the diameter D, gravitational acceleration g and the surrounding liquid density ρ_l. The non-dimensional variables are the spatial coordinates $x_i^* = x_i/D$, velocity $u_i^* = u_i/\sqrt{gD}$, time $t^* = t/\sqrt{D/g}$, pressure $p^* = p/(\rho_l g D)$ and the bubble interface curvature $\kappa^* = \kappa D$.

The non-dimensional governing equations for the two-phase flow are

$$\frac{\partial u_i^*}{\partial x_i^*} = 0\,, \tag{A.1}$$

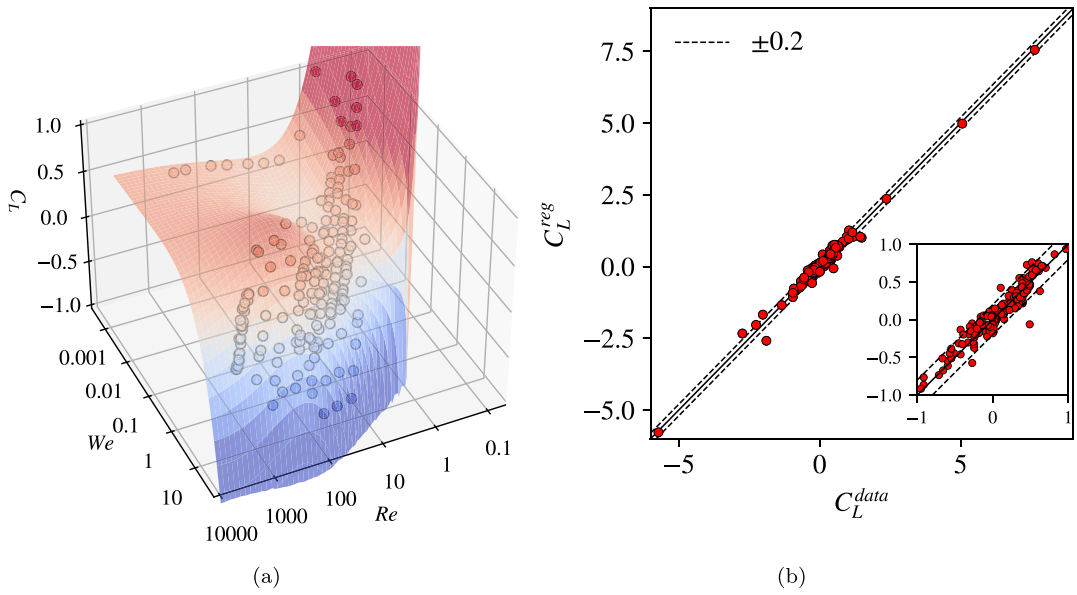

Fig. B.1. (a): 3D-view of the included data points and the fitted surface $C_L^{reg}(Re, We)$ (Eq. (B.2)) coloured by the C_L-value. (b): Comparison of the predicted $C_L^{reg}(Re, We)$ to the C_L^{data} obtained from the literature.

$$\rho^*\left(\frac{\partial u_i^*}{\partial t^*} + u_j^*\frac{\partial u_i^*}{\partial x_j^*}\right) = \rho^* g_i^* - \frac{\partial p^*}{\partial x_i^*} + \frac{1}{Ga}\frac{\partial}{\partial x_j^*}\left(\mu^*\left(\frac{\partial u_i^*}{\partial x_j^*} + \frac{\partial u_j^*}{\partial x_i^*}\right)\right) + \frac{\kappa^*\delta_S^* n_i}{Eo}, \tag{A.2}$$

$$\frac{\partial c}{\partial t^*} + \frac{\partial c u_i^*}{\partial x_i^*} = 0, \tag{A.3}$$

where c is the volume fraction of liquid and the non-dimensional density ρ^* and viscosity μ^* fields are defined as

$$\rho^*(c) = c + (1-c)/\rho_r, \tag{A.4}$$

$$\mu^*(c) = \left(c + (1-c)\mu_r\right)^{-1}. \tag{A.5}$$

The bubble is initialized as a sphere with diameter $D^* = 1$ and the undisturbed liquid shear flow is prescribed as $U_y^* = -x^* Sr$. In total, we thus get following set of five dimensionless (input) parameters that completely describes the present problem:

$$Ga = \frac{\rho_l\sqrt{gD}D}{\mu_l}, Eo = \frac{\rho_l g D^2}{\sigma}, Sr = \frac{|\omega_\infty|D}{\sqrt{gD}}, \rho_r = \frac{\rho_l}{\rho_g}, \mu_r = \frac{\mu_l}{\mu_g}. \tag{A.6}$$

Appendix B. Lift force model in the $Re - We$ phase-space

We provide an additional regression model for C_L based on the Re and We-numbers using the same dataset and methodology as outlined in Section 4. Here, the value of $We = 0.001$ is used to represent the results of Legendre and Magnaudet (1998) for spherical bubbles. The set of (Re, We) becomes the governing parameters if the problem is non-dimensionalized using $(\rho_l, |\overline{V}_r|, D)$ (instead of (ρ_l, g, D) used in Appendix A). Since $|\overline{V}_r|$ is typically not known a priori, these governing parameters are less convenient than the set of (Ga, Eo) used in Section 4. The (Re, We)-numbers are however more conventional in, for example, CFD-codes and the model $C_L^{reg}(Re, We)$ may therefore also be useful. The regression model reads

$$C_L^{reg}(Re, We) = \tag{B.1}$$

$$\frac{-13 - 58y - 28y^2 - 6y^3 + 13x + 61xy + 8xy^2 + 5x^2 - 23x^2y - x^3}{14.3 - 49y - 32y^2 - 6.9y^3 + 39x + 64.6xy + 23.7xy^2 - 33x^2 - 24.5x^2y + 9.3x^3} \tag{B.2}$$

where $x = \log_{10}(Re)$ and $y = \log_{10}(We)$. The absolute standard deviation is $\sigma_{C_L} = 0.12$ and the coefficient of determination $R^2 = 0.98$ between the regression model and the data points. This model shows the same characteristics and similar, but slightly worse, accuracy (compared to the dataset) as the model Eq. (10) developed for the (Ga, Eo) phase-space. The $C_L^{reg}(Re, We)$-surface in the relevant ranges of the governing parameters is shown in Fig. B.1(a) and a comparison of the predicted C_L-values to the dataset is provided in Fig. B.1(b). Here, both figures show a good agreement with the dataset and similar trends as $C_L^{reg}(Ga, Eo)$ in Section 4. The model is considered relevant within the approximate parameter boundaries $Re \geq 0.1, We < 1.6Re^{0.9}, We < 30$. Outside these boundaries, the steep slope of $C_L^{reg}(Re, We)$ and the lack of data points makes the model less accurate.

Data availability

Data will be made available on request.

References

Adoua, R., Legendre, D., Magnaudet, J., 2009. Reversal of the lift force on an oblate bubble in a weakly viscous linear shear flow. J. Fluid Mech. 628, 23–41.

Aoyama, S., Hayashi, K., Hosokawa, S., Lucas, D., Tomiyama, A., 2017. Lift force acting on single bubbles in linear shear flows. Int. J. Multiph. Flow 96, 113–122.

Auton, T., 1987. The lift force on a spherical body in a rotational flow. J. Fluid Mech. 183, 199–218.

Bunner, B., Tryggvason, G., 2002. Dynamics of homogeneous bubbly flows Part 1. Rise velocity and microstructure of the bubbles. J. Fluid Mech. 466, 17–52.

Cano-Lozano, J., Bohorquez, P., Martínez-Bazán, C., 2013. Wake instability of a fixed axisymmetric bubble of realistic shape. Int. J. Multiph. Flow 51, 11–21.

Cano-Lozano, J.C., Martinez-Bazan, C., Magnaudet, J., Tchoufag, J., 2016. Paths and wakes of deformable nearly spheroidal rising bubbles close to the transition to path instability. Phys. Rev. Fluids 1 (5), 053604.

Dijkhuizen, W., van Sint Annaland, M., Kuipers, J., 2010. Numerical and experimental investigation of the lift force on single bubbles. Chem. Eng. Sci. 65 (3), 1274–1287.

Drew, D., Lahey, R., 1987. The virtual mass and lift force on a sphere in rotating and straining inviscid flow. Int. J. Multiph. Flow 13 (1), 113–121.

Ertekin, E., Kavanagh, J.M., Fletcher, D.F., McClure, D.D., 2021. Validation studies to assist in the development of scale and system independent CFD models for industrial bubble columns. Chem. Eng. Res. Des. 171, 1–12.

Feng, J., Bolotnov, I.A., 2017. Interfacial force study on a single bubble in laminar and turbulent flows. Nucl. Eng. Des. 313, 345–360.

Hayashi, K., Hessenkemper, H., Lucas, D., Legendre, D., Tomiyama, A., 2021. Scaling of lift reversal of deformed bubbles in air-water systems. Int. J. Multiph. Flow 142, 103653.

Hayashi, K., Legendre, D., Tomiyama, A., 2020. Lift coefficients of clean ellipsoidal bubbles in linear shear flows. Int. J. Multiph. Flow 129, 103350.
Hessenkemper, H., Ziegenhein, T., Rzehak, R., Lucas, D., Tomiyama, A., 2021. Lift force coefficient of ellipsoidal single bubbles in water. Int. J. Multiph. Flow 138, 103587.
Hidman, N., Ström, H., Sasic, S., Sardina, G., 2022. The lift force on deformable and freely moving bubbles in linear shear flows. J. Fluid Mech. 952, A34.
Lee, W., Lee, J.-Y., 2020. Experiment and modeling of lift force acting on single high Reynolds number bubbles rising in linear shear flow. Exp. Therm. Fluid Sci. 115, 110085.
Legendre, D., Magnaudet, J., 1997. A note on the lift force on a spherical bubble or drop in a low-Reynolds-number shear flow. Phys. Fluids 9 (11), 3572–3574.
Legendre, D., Magnaudet, J., 1998. The lift force on a spherical bubble in a viscous linear shear flow. J. Fluid Mech. 368, 81–126.
Lucas, D., Krepper, E., Liao, Y., Rzehak, R., Ziegenhein, T., 2020. General guideline for closure model development for gas-liquid flows in the multi-fluid framework. Nucl. Eng. Des. 357, 110396.
Lucas, D., Krepper, E., Prasser, H.-M., 2001. Prediction of radial gas profiles in vertical pipe flow on the basis of bubble size distribution. Int. J. Therm. Sci. 40 (3), 217–225.
Lucas, D., Prasser, H.-M., Manera, A., 2005. Influence of the lift force on the stability of a bubble column. Chem. Eng. Sci. 60 (13), 3609–3619.
Lucas, D., Tomiyama, A., 2011. On the role of the lateral lift force in poly-dispersed bubbly flows. Int. J. Multiph. Flow 37 (9), 1178–1190.
Mazzitelli, I.M., Lohse, D., 2009. Evolution of energy in flow driven by rising bubbles. Phys. Rev. E 79 (6), 066317.
McLaughlin, J.B., 1991. Inertial migration of a small sphere in linear shear flows. J. Fluid Mech. 224, 261–274.
Mudde, R.F., 2005. Gravity-driven bubbly flows. Annu. Rev. Fluid Mech. 37, 393–423.
Saffman, P., 1965. The lift force on a small sphere in a slow shear flow. J. Fluid Mech. 22, 385–400.
Tomiyama, A., Tamai, H., Zun, I., Hosokawa, S., 2002. Transverse migration of single bubbles in simple shear flows. Chem. Eng. Sci. 57 (11), 1849–1858.
Tripathi, M.K., Sahu, K.C., Govindarajan, R., 2014. Why a falling drop does not in general behave like a rising bubble. Sci. Rep. 4, 4771.
Ziegenhein, T., Tomiyama, A., Lucas, D., 2018. A new measuring concept to determine the lift force for distorted bubbles in low morton number system: Results for air/water. Int. J. Multiph. Flow 108, 11–24.
Ẑun, I., 1980. The transverse migration of bubbles influenced by walls in vertical bubbly flow. Int. J. Multiph. Flow 6 (6), 583–588.